Temporal scaling behavior of decaying two-dimensional turbulence

Jeffrey B. Weiss and James C. McWilliams
National Center for Atmospheric Research, P.O. Box 3000, Boulder, Colorado 80307

(Received 20 February 1992; accepted 16 October 1992)

Decaying two-dimensional turbulence is characterized by the emergence of coherent vortices, which subsequently dominate the evolution. The temporal scaling behavior of the flow is analyzed using a scaling theory, a long-time integration of the fluid equations, and a dissipative, modified point-vortex model that represents the turbulence as a system of interacting coherent structures. Good agreement is found in the behavior of average vortex properties, low-order moments of the flow fields, and the form of self-similar evolution.

I. INTRODUCTION

Two-dimensional turbulence has been the subject of much research in recent years, both because it is a paradigm for anisotropic geophysical and astrophysical turbulence and because it is the most computationally accessible example of fluid turbulence. High-resolution numerical simulations[1–5] and a new scaling theory[6] have greatly clarified our understanding of decaying two-dimensional turbulence and the role of coherent vortices. The decay of the system from random initial conditions can be divided into three stages. In the first stage, the fluid self-organizes into a collection of coherent vortices containing most of the surviving vorticity. Once the coherent vortices have emerged, the second stage begins, during which the coherent vortices dominate the evolution. In this stage, the evolution is governed primarily by two processes: (1) nearly conservative mutual advection of the vortices when they are well separated and (2) dissipative interaction of vortices when they become close. The resulting evolution exhibits scaling behavior, in that aggregate measures of both the flow fields and the vortex population evolve algebraically,[3] with exponents that are simply related.[6] As the evolution proceeds, the number of vortices decreases, until a final state consisting of a single pair of opposite-sign vortices, a dipole, is achieved.[4,7] At this point, the nonlinear contribution to the dissipative evolution ceases, and the final stage begins in which the dipole decays diffusively.

In this paper, we shall explore the scaling regime of the middle stage of the evolution by concentrating on the coherent vortices. The result is a picture of turbulence as a system of interacting coherent structures including both chaotic dynamics and intermittent dissipation, rather than the more traditional picture of turbulence as a random velocity field. In exploring this conception of turbulence we shall explicitly construct a model of interacting vortices, which, although extremely simple, captures many of the essential features of the turbulence.

The fluid dynamical equations in terms of the vorticity are

$$\zeta_t + J(\psi,\zeta) = (-1)^{p+1}\nu_p \nabla^{2p}\zeta, \quad \zeta \equiv \nabla^2\psi, \tag{1}$$

where $\psi(x,y)$ is the streamfunction, $\zeta = (\nabla \times \mathbf{u})\cdot\hat{z}$ is the vorticity, $\mathbf{u}$ is the velocity, $J(a,b) \equiv a_x b_y - a_y b_x$ is the Jacobian, and ν_p is the viscosity where $p=1$ for ordinary viscosity and $p \geqslant 2$ for hyperviscosity (our solution below has $p=2$). The nonlinearity of the flow is characterized by the Reynolds number, $\mathrm{Re} \propto 1/\nu_p$; our interest here will be flows with large Re. The fluid evolves in a doubly periodic square domain with side $2\pi L$.

The relevant aggregate measures of the flow fall into two categories: low-order, spatially averaged moments of the flow fields and properties of the vortex population. We shall focus on three low-order, spatially averaged moments: the kinetic energy per unit area E, the enstrophy Z, and the vorticity kurtosis K,

$$E = \frac{1}{(2\pi L)^2}\int d\mathbf{x}\,\frac{|\mathbf{u}|^2}{2},$$

$$Z = \frac{1}{(2\pi L)^2}\int d\mathbf{x}\,\zeta^2, \tag{2}$$

$$K = \frac{1}{Z^2}\frac{1}{(2\pi L)^2}\int d\mathbf{x}\,\zeta^4.$$

Experience, and in some instances, rigorous mathematical arguments, show the following behavior for large Re: E is conserved, Z is dissipated, and K, a measure of the intermittency, grows as the coherent vortices develop and evolve.[2,8–10] The enstrophy decreases through the dissipation of vorticity filaments that are generated by close interaction of coherent vortices. These filaments are stretched to ever smaller scales by the turbulent strain field, until they reach the dissipation scale, where they are diffused away. Since the total energy of the fluid is conserved while the filaments are dissipated, it follows that they carry no energy, leaving all the energy in the coherent vortices. The manner in which the energy is partitioned among the evolving structures is discussed in Sec. V.

The vortex properties of interest are the total number of vortices N, the average radius r_a, the average circulation magnitude Γ_a, the average vorticity amplitude of the vortex cores ζ_a, and their distribution functions. The characteristics of the emergent vortex population depend on the energy wave number spectrum of the random initial condition through the process of vortex self-organization during the first stage of evolution. Relatively broadband spectra give rise to a population with a wide distribution of sizes,[11] while narrow-band spectra produce a relatively narrow distribution.[3] We shall focus here on the latter case,

 0899-8213/93/030608-14$06.00

where the narrow distribution of vortex properties can be meaningfully described by average quantities. In the case of broadband spectra, the initial distribution of vortex sizes has a band-limited, power-law form, and average quantities are less useful.

In a recent paper with our colleagues,[6] we proposed a new scaling theory for the evolution during the second stage, after vortex emergence but before formation of the final dipole. In this theory the quantities of interest display scaling behavior in which the time dependence is algebraic and the exponents are all given in terms of a single undetermined exponent, ξ. The paper also contained preliminary confirmations of the scaling theory by both a high-resolution turbulence solution and a modified point-vortex model. A recent experiment in thin layers of electrolyte also confirms the scaling theory.[12]

In this paper we both extend the work of our previous paper[6] and test the scaling theory in significantly greater detail. We show how scaling theory implicitly assumes self-similar evolution of probability distributions of vortex properties, and introduce finite Reynolds number corrections to the theory. We integrate the turbulence solution three times longer and the modified point-vortex model 20 times longer than previously, the latter improvement made possible by a new renormalization technique. In addition, we improve the modified point-vortex model by incorporating a new critical merger distance appropriate for vortices with different sizes, obtained by studying the elliptical-moment model. Finally, we construct a new energy partition appropriate for structured flows, and assess the energy evolution in the modified point-vortex model.

II. SCALING THEORY

The classical proposal for self-similar spectrum evolution[8] is based on the idea that the only conserved quantity is the energy, and it predicts that the enstrophy decays as t^{-2}. Numerical solutions, however, indicate that the emergence of coherent vortices significantly slows the enstrophy decay.[3,4,13] In addition, a second conserved quantity appears: the vorticity amplitude inside the vortex cores ζ_e, which is shielded from the deformation, cascade, and dissipation that occurs on the edges of and outside the vortices.[5,9,14–16] We use the two conserved quantities, E and ζ_a, the population average of ζ_e, to construct a scaling theory for the evolution of both vortex properties and statistical moments of the fields. The conservation of E and ζ_a can only be expected to be valid as $\mathrm{Re}\to\infty$; the scaling theory is thus an infinite-Re theory. However, it is not a conservative theory, as no other inviscid invariants are preserved.

In the scaling theory, the vortex population is characterized by N, r_a, and ζ_a; thus scaling theory is a "mean-vortex" theory. By assuming that all the vorticity is concentrated in the vortices, one can express the scaling behavior of the other properties in terms of these three quantities:

$$\Gamma_a\sim\zeta_a r_a^2,\quad Z\sim N\zeta_a^2 r_a^2,\quad K\sim\frac{1}{(Nr_a^2)},\quad E\sim N\zeta_a^2 r_a^4, \tag{3}$$

where the scaling for E is obtained by ignoring possible logarithmic corrections. The issue of logarithmic corrections is explored more fully in Sec. V.

The conserved properties,

$$E(t)=E(t_0),\quad \zeta_a(t)=\zeta_a(t_0), \tag{4}$$

where t_0 is any time within the scaling regime, together with the algebraic evolution of vortex number observed in turbulence solutions,[3]

$$N(t)=N(t_0)\left(\frac{t}{t_0}\right)^{-\xi}, \tag{5}$$

provide the three elements necessary to close the theory. The evolution of the other properties is then

$$\begin{aligned} r_a(t)&=r_a(t_0)\left(\frac{t}{t_0}\right)^{\xi/4},\quad \Gamma_a(t)=\Gamma_a(t_0)\left(\frac{t}{t_0}\right)^{\xi/2},\\ Z(t)&=Z(t_0)\left(\frac{t}{t_0}\right)^{-\xi/2},\quad K(t)=K(t_0)\left(\frac{t}{t_0}\right)^{\xi/2}. \end{aligned} \tag{6}$$

Thus, the evolution of all relevant quantities is algebraic, and the exponents can be expressed in terms of ξ. While our focus here is on the regime where there is a relatively large number of vortices, we note that the scaling theory can be extrapolated down to the final dipole to provide predictions about the end state of the nonlinear evolution.[7]

The scaling theory addresses the evolution of average properties, under the assumption that averages of powers of quantities scale the same as powers of averages, e.g.,

$$\overline{r^\mu(t)}=c_\mu[\overline{r(t)}]^\mu, \tag{7}$$

where c_μ is independent of time and the symbol $\bar{}$ indicates an average over the vortex population at a given time, e.g., $r_a(t)\equiv\overline{r(t)}$. The vortex population is fully described by a probability distribution function ρ, which is a function of the vortex size, shape, and vorticity amplitude. The assumption (7) requires that ρ evolve self-similarly. If, for simplicity, we consider only the dependence on vortex size, then the scaling assumption (7),

$$\int dr\, r^\mu\rho(r,t)=c_\mu\left(\int dr\, r\rho(r,t)\right)^\mu, \tag{8}$$

is equivalent to assuming self-similar evolution of ρ,

$$\rho(r,t)dr=p\left(\frac{r}{r_a(t)}\right)\frac{dr}{r_a(t)}=p(x)dx, \tag{9}$$

for some function p and $x=r/r_a(t)$. Thus, self-similar evolution results in the distribution $p(x)$ being independent of time. We use the normalization $\int\rho(r,t)dr=\int p(x)dx=1$. The generalizations to shape and amplitude dependence are straightforward.

III. TURBULENCE SOLUTIONS

We shall examine a particular high-resolution, long-duration solution of (1) for its temporal scaling behavior. This solution is an extension in time, by nearly a factor of 4 to $t=150$, of the solution analyzed extensively in previous papers.[3,6,7] It is a pseudospectral numerical integration

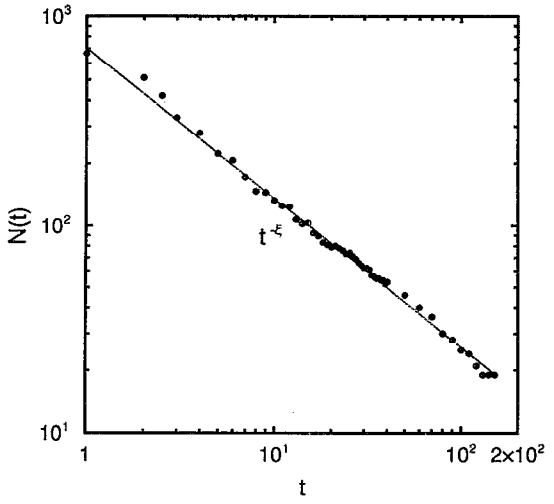

FIG. 1. The vortex population in the turbulence solution and the comparison curve from scaling theory (5) with $\xi=0.72$.

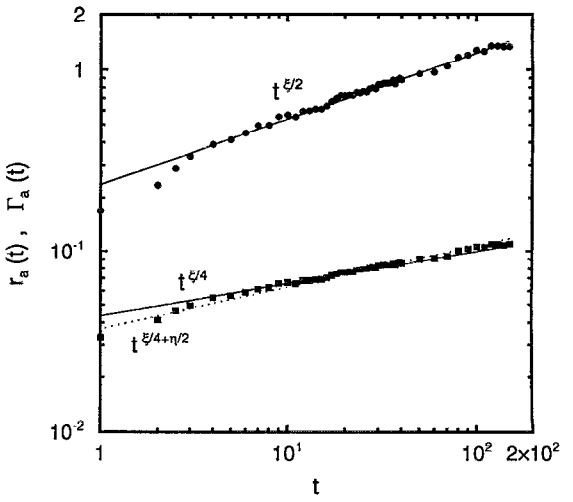

FIG. 2. The average vortex size (squares) and circulation (circles) in the turbulence solution and comparison curves (solid lines) from scaling theory (6) with $\xi=0.72$. The dotted line is the finite-Re correction to the vortex size (11) with $\eta=0.1$.

with domain size $L=1$ and hyperviscosity $\nu_2=3.5\times10^{-9}$. Its initial conditions have energy $E(0)=0.5$, spectrum peak wave number $k_0=30$, eddy-circulation time $Z(0)^{-1/2}=0.021$, and vorticity kurtosis $K(0)=3.0$ (consistent with random-phase initialization). The spatial grid resolution is 450 intervals in each coordinate direction.

The first stage of evolution, comprising the maximum of enstrophy dissipation at $t\approx0.25$ and the emergence of the coherent vortices, is essentially completed by $t=1$ when $E(1)=0.464$, $Z(1)^{-1/2}=0.041$, and $K(1)=6.4$. Our analysis here will be restricted to the interval $1\leqslant t\leqslant150$, which spans approximately 1000 eddy-circulation times. This interval comprises only part of the second stage of evolution; an estimate from scaling theory[7] for the end of the second stage for this solution is $t\approx3500$, which is beyond our means (given our ends).

The population of coherent vortices is analyzed by an automated vortex census[3] that tests the local vorticity patterns based on an idealization of coherent vortex structure as axisymmetric and monotonically decreasing away from the central extremum. Patterns are selected as vortices if they approximately fit this form. The properties of each of the selected vortices are then measured; here we will focus on the radius r_i (equal to the square root of the vortex area divided by π), circulation Γ_i, and central extremum ζ_{e_i} of vortex i.

Figure 1 shows the total number of vortices $N(t)$ from the turbulence solution, together with the scaling form (5) with $\xi=0.72$. Except for sampling fluctuations of modest amplitude, it conforms quite well to algebraic decay over the lengthy interval in which the vortex population decreases by nearly a factor of 35. The trend in Fig. 1 is reasonably well fit by $\xi\approx0.70$–0.75; the particular value $\xi=0.72$ is chosen for consistency with the results of Sec. IV.

Figure 2 shows $r_a(t)=\overline{r_i(t)}$ and $\Gamma_a(t)=\overline{|\Gamma_i(t)|}$ and their scaling forms (6). The correspondence with scaling theory is quite good over most of the interval, although there is some indication that an adjustment to scaling behavior is still occurring up to a time of 3 or 4. From the previous analysis,[3] we can associate this with a transient phase in which there is a relatively large fraction of small, weak vortices in the population, compared to later times.

The average vorticity amplitude $\zeta_a(t)=\overline{|\zeta_{e_i}(t)|}$ in Fig. 3 also exhibits this transient phase. Thereafter it corresponds reasonably well with the scaling theory assumption (4), although there is a discernible downward trend. An approximate algebraic fit, $t^{-\eta}$, to this later trend yields an exponent of $\eta\approx0.1$. This is almost certainly an indication that the small but finite viscosity has a measurable influence over the lengthy integration time here. It acts

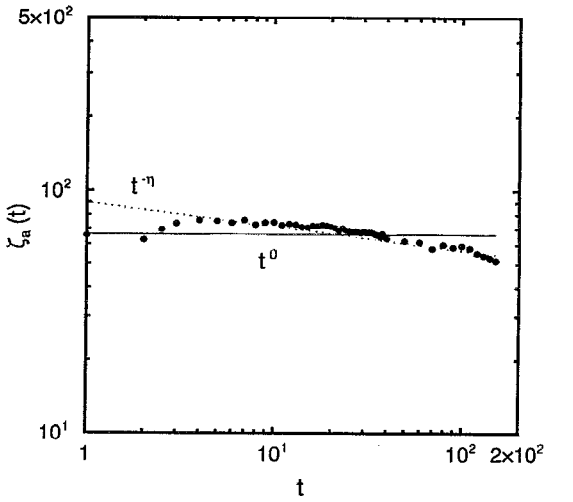

FIG. 3. The average vortex amplitude in the turbulence solution and the comparison curve (solid line) from scaling theory (4). The dotted line is the finite-Re correction to the vortex amplitude (10) with $\eta=0.1$.

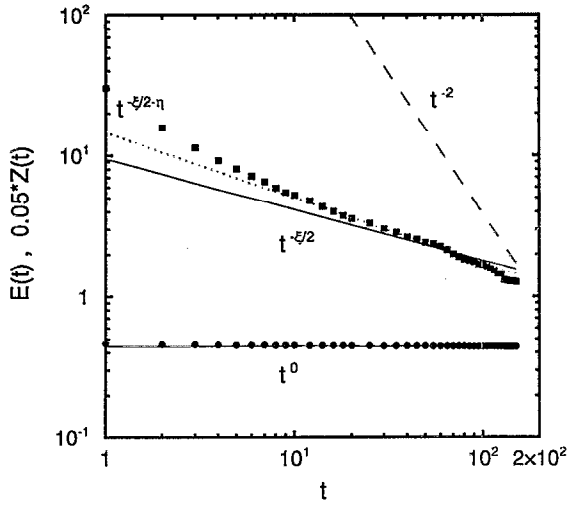

FIG. 4. The energy (circles) and 0.05 times the enstrophy (squares) in the turbulence solution, comparison curves from scaling theory, (4) and (6) with $\xi=0.72$ (solid lines), and the classical proposal[8] for self-similar evolution (dashed line). The dotted line is the finite-Re correction to the enstrophy (11) with $\eta=0.1$.

diffusively to reduce the vorticity extrema and represents a finite-Re departure from the infinite-Reynolds-number scaling theory.

The second moments $E(t)$ and $Z(t)$ are shown in Fig. 4. The energy corresponds very well with the scaling-theory assumption (4), but, even after the initial transient phase, the enstrophy shows a greater rate of decay than in (6). Again we attribute the discrepancy to the finite Re of the turbulence solution. On the other hand, the decay rate is clearly much closer to the scaling theory than the classical $\mathrm{Re}=\infty$ proposal[7] of t^{-2}. The normalized fourth moment, $K(t)$ in Fig. 5, conforms quite well with the scaling theory (6), but it also exhibits the same initial transient as

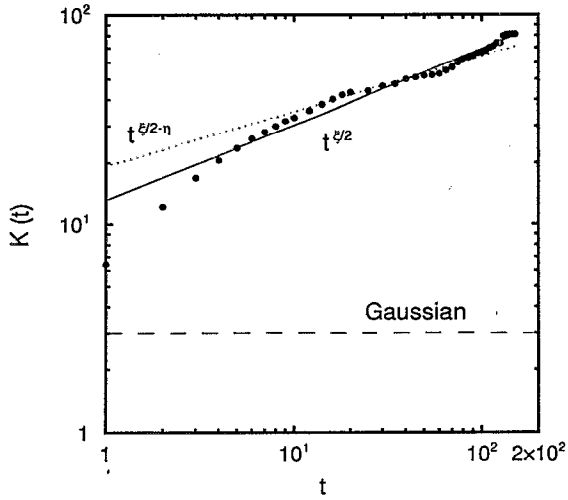

FIG. 5. The vorticity kurtosis in the turbulence solution and the comparison curve (solid line) from scaling theory (6) with $\xi=0.72$. The dotted line is the finite-Re correction (11) with $\eta=0.1$.

well as appreciable sampling variability (i.e., oscillations about algebraic growth) on a long time scale.

In summary, the average properties of the vortex population and low-order statistical moments correspond rather well to the scaling theory predictions, albeit with the following qualifications: there is an early period of adjustment to the regime of scaling behavior; there is evident sampling variability associated with the finite population size, with differing magnitudes for different quantities; and there are somewhat greater decay rates for vorticity extrema and enstrophy that we attribute to the finite Re of the turbulence solution.

We can attempt a quantitative rationalization of the diffusive influences by modifying the scaling theory predictions to include decay of ζ_a and growth of r_a in such a way as to preserve Γ_a. This is an exact property of the axisymmetric conduction equation for ζ and we can use it as a hypothesis for including finite-Re effects of (1). Under this hypothesis, the scaling forms are unaltered from (4)–(6) for E, N, and Γ, all of which fit quite well the turbulence solution in Figs. 1, 2, and 4. However, if we assume a diffusive effect,

$$\zeta_a \propto t^{-\eta}, \tag{10}$$

and conservation of Γ_a under diffusion, then from (3),

$$r_a \propto t^{\xi/4+\eta/2}, \quad Z \propto t^{-\xi/2-\eta}, \quad K \propto t^{\xi/2-\eta}. \tag{11}$$

If we take $\eta=0.1$ (as a fit to Fig. 3; see above), then we note that all the corrections in (11) are relatively small, and presumably vanish as $\mathrm{Re}\to\infty$.

We see from Fig. 2 that the best exponent for r_a lies in between (6) and (11). From Fig. 4 we see that the best exponent for Z is even a little more negative than (11), but clearly more so than (6). From Fig. 5 we see that the best exponent for K appears closer to (6) than to (11), although the sampling variability precludes a clear distinction. We conclude that although we are not able to confirm the diffusive corrections (10) and (11) with great precision, they do have the correct sense and magnitude. Because these corrections are relatively small, we will return to the $\mathrm{Re}=\infty$ scaling theory for the remainder of the paper.

An earlier analysis of this solution[3] calculated the distribution function of vortex amplitude. Here we shall focus on the probability distribution function of vortex size $\rho(r,t)$. These two single-property distribution functions would completely describe their joint distribution function if they were independent. In fact, the present solution, with narrow-band initial condition, shows only a weak correlation, in that the smallest few vortices have weaker amplitudes than average. This approximate independence of the single-property distributions is also seen in solutions with broadband initial conditions.[11] A further reason to focus here on $\rho(r,t)$ is that it allows direct comparison with the modified point-vortex model of Sec. IV.

Scaling behavior is intimately linked to self-similar evolution of the probability distribution function for vortex properties (Sec. II). Thus, we investigate the hypothesis that $\rho(r,t)$ evolves self-similarly as in (9), using the

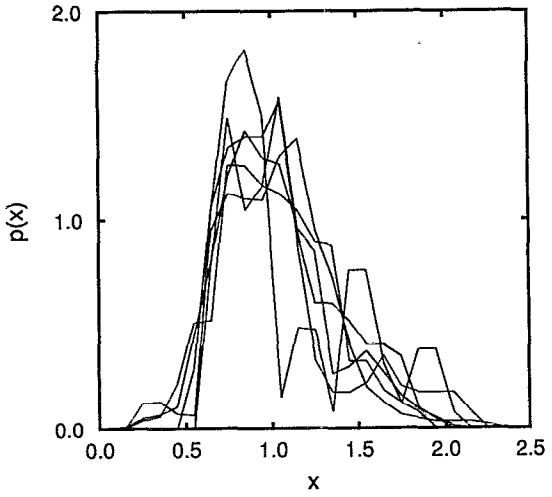

FIG. 6. The instantaneous vortex size distribution function $p(x)$ (9) from the turbulence solution at $t=4$, 8, 15, 30, 60, and 120.

scaling-theory form (6) for r_a with $r_a(t_0)$ chosen to match the turbulence solution at $t_0=10$. Figure 6 shows several instantaneous evaluations of $p(x)$, based upon the vortex census. There is evidently considerable sampling variability in the instantaneous distributions, but there is no evident trend, consistent with the hypothesis of self-similarity. In a time average of the instantaneous distributions, Fig. 7, the sampling variability is substantially reduced and a smooth distribution results.

IV. MODIFIED POINT-VORTEX MODEL

Our goal in this section is to construct the simplest model that captures the essential phenomena of the scaling regime of two-dimensional decaying turbulence. The degree of success of this model will be a measure of our understanding of the essential dynamics underlying the phenomena. The model we describe here is a modification of the one we used previously.[6] While we shall be concerned here with the case where the vortices emerge from narrow-band random initial conditions, we note that Benzi *et al.*[17] independently devised a model identical to our previous one to study the broadband case.

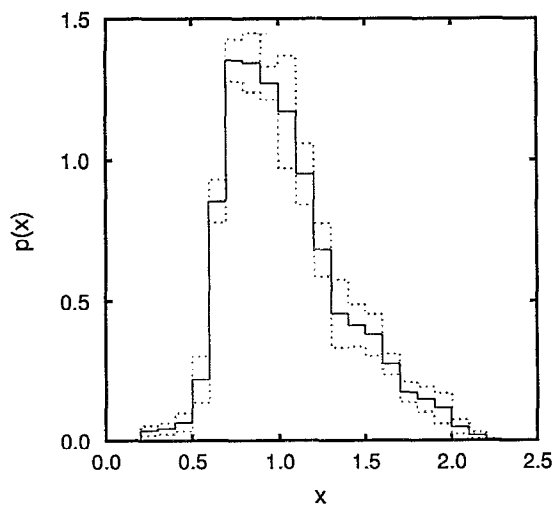

FIG. 7. The average vortex size distribution function $p(x)$ (9) from the turbulence solution, averaged over the times in Fig. 6. The uncertainty (dotted curve) is estimated by the standard error of the mean, assuming the six times are independent.

We now give a brief overview of our rationale for the model's design. Our goal of using the simplest possible model means that we shall represent the coherent vortices with a minimal number of degrees of freedom. The minimal representation is as point vortices, whose invariant circulations Γ_i completely determine the velocity field. This representation is appropriate when coherent vortices are far apart, and they move under their mutual advection.[11,18] Representing dissipative interactions of close vortices, parametrized here by abrupt transformations, requires consideration of the size of the vortices. Thus we increase the complexity of the representation and consider uniform circular disks with radius r_i and, thus, vorticity $\zeta_i=\Gamma_i/\pi r_i^2$. The criterion for triggering an abrupt transformation, mimicking vortex merger, is separation of like-sign vortices by no more than a critical distance d_c. The determination of d_c involves shape deformations for which the simplest representation is uniform elliptical patches. We find that this is the maximum complexity we need to construct the model. Our approach of using a single-point/disk/elliptical vortex for a single coherent vortex should be contrasted with more complex approaches, such as using many point or blob vortices or a few isovorticity contours to represent the continuously distributed vorticity field within each coherent vortex.[19,20]

The dynamics of point vortices is Hamiltonian,[21]

$$\Gamma_i\begin{pmatrix}\dot{x}_i\\ \dot{y}_i\end{pmatrix}=\begin{pmatrix}\dfrac{\partial H}{\partial y_i}\\ -\dfrac{\partial H}{\partial x_i}\end{pmatrix},\quad \dot{\Gamma}_i=0, \tag{12}$$

where vortex i has position (x_i,y_i) and circulation Γ_i. In a square periodic domain H takes the form[22]

$$H(\{x_i,y_i,\Gamma_i\})=-\sum_{i,j,i\neq j}\frac{\Gamma_i\Gamma_j}{2}G(x_i-x_j,y_i-y_j), \tag{13}$$

where

$$G(x,y)=\frac{1}{4\pi}\left[\sum_{m=-\infty}^{\infty}\ln\left(\frac{\cosh(x/L-2\pi m)-\cos(y/L)}{\cosh(2\pi m)}\right)-\frac{x^2}{2\pi L^2}\right]-G_c, \tag{14}$$

and G_c is an arbitrary constant that we are free to add to G. It is convenient to choose

$$G_c=\frac{1}{12}-\frac{1}{4\pi}\ln 2-\frac{1}{2\pi}\sum_{m=1}^{\infty}\ln(1+e^{-4\pi m})=0.028\ 17..., \tag{15}$$

which results in $\int d\mathbf{x}\, G(\mathbf{x})\equiv 0$.[23] The sum in (14) converges rapidly, and can be usefully truncated for numerical

computations. If $N>3$, the Hamiltonian (13) is nonintegrable and the dynamics is chaotic.

Point-vortex dynamics, being Hamiltonian, is conservative. In addition to H, the dynamics conserves the vortex momentum,

$$\mathbf{P}\equiv\sum_i \Gamma_i(y_i\hat{x}-x_i\hat{y}). \tag{16}$$

(See Ref. 22 for more details about **P**.) For small but finite disks evolving under point-vortex dynamics, the total energy is conserved (see Sec. V), as are all moments of the vorticity field.

In two-dimensional turbulence, dissipation becomes important when two vortices approach closely, and thus some modification of point-vortex dynamics is required. While the dissipative interaction of two vortices can be quite complex, for simplicity we only include what we assert to be the most important phenomenon: merger of same-sign vortices. When two same-sign point vortices become closer than some critical merger distance, d_c, the Hamiltonian dynamics is interrupted, the two vortices are replaced by a single new vortex, and the Hamiltonian dynamics continues with this new set of vortices.

The properties of the new vortex are determined from transformation rules based on representing the vortices as uniform disks and conserving the same properties as the scaling theory: energy and peak vorticity. In this paper we shall restrict ourselves to initial vortex populations with uniform vorticity: $\zeta_i=\pm\zeta_a$ for all i. In this context, conservation of peak vorticity implies that when two same-sign vortices, 1 and 2, merge to form vortex 3,

$$\zeta_3=\zeta_1=\zeta_2\,. \tag{17}$$

In the scaling theory, the energy is related to the average vortex properties by (3), where possible logarithmic corrections have been ignored. Here we hypothesize that (3) is also true for individual vortices; we discuss the validity of this hypothesis in Sec. V. Together with the transformation rule for vorticity (17), this results in the transformation rule for vortex size,

$$r_3^4=r_1^4+r_2^4. \tag{18}$$

In principle, these rules could be extended to populations with unequal vorticity amplitudes. All other invariants of the Hamiltonian system apart from the explicitly conserved quantities are lost in the transformation, including total circulation and enstrophy.

Our model fits into a general framework of punctuated Hamiltonian dynamics, where Hamiltonian evolution is punctuated by dissipative events. These events, represented mathematically by abrupt transformations of the Hamiltonian system, characterize the outcome of an irreversible evolution toward local flow complexity ending in dissipation. The onset of irreversible behavior occurs on a time scale fast compared to the intervortex Hamiltonian evolution in (12), and is thus represented as an instantaneous transformation. While we discuss here only the simplest of such models, and only for two-dimensional decaying turbulence, we feel that this general class of dynamical systems is potentially well suited to modeling any turbulent flow that develops sufficiently coherent structuring of the vorticity field.[24]

A. Critical merger distance

Two identical initially circular vortices merge when their initial separation is less than approximately 3.3 times the vortex radius.[15] In our previous paper[6] and in Benzi *et al.*,[17] the criterion $d_c=3.3(r_1+r_2)/2$ was used for all vortex mergers. Using the elliptical-moment model,[25] we develop an alternative criterion more appropriate for unequal vortices.

The elliptical-moment model, in which the vortices are represented as elliptical patches of uniform vorticity in an open domain, is the simplest model that exhibits a phenomenon analogous to vortex merger.[15] Since the vortices are assumed to remain elliptical, the model cannot capture the filamentation and entanglement of vorticity that actually occurs in vortex merger. It does, however, contain the phenomenon of vortex collapse, in which the distance between the centroids of two vortices goes to zero while the ellipticities of the vortices grow. Vortex collapse thus captures the early stages of vortex merger. Identifying the threshold for vortex collapse with that for vortex merger allows us to use the elliptical-moment model to calculate a critical merger distance for unequal vortices.

In the Appendix we study the nonlinear dynamics of the elliptical-moment model in some detail. In particular, we focus on the collapse of two initially circular vortices with equal uniform vorticity and radii r_1 and r_2. We find that the collapse boundary is well fit by a simple curve,

$$d_c(r_1,r_2)=2.592r_2+0.609\frac{r_1^2}{r_2},\quad r_1<r_2\,. \tag{19}$$

We note that this agrees with previously obtained results for the case $r_1=r_2$.[15]

The true complexity of vortex interactions is, of course, enormous. Even a gross simplification such as the elliptical-moment model exhibits the complexity of Hamiltonian chaos. As one goes further along the hierarchy toward more realistic models, the complexity increases. Using contour dynamics to model vortices with uniform vorticity, Dritschel and Waugh find that the results of vortex interaction depend in a complicated manner on the initial sizes and separations.[26] The boundary they find between conservative and dissipative interactions is, however, close to the d_c found in the moment model. If one wants to model vortex interactions more realistically, one would have to go even further and include continuous vorticity profiles. Furthermore, to realistically model vortex interactions in a turbulent fluid, one would also need to include the fluctuating strain field associated with the chaotic motions of other, distant vortices.

Our approach here, however, is to test our understanding of turbulence using the simplest relevant model. An important aspect of our simplification is a binary declaration about the dissipative close interaction of two vortices: either it is wholly conservative or the vortices merge completely without loss of Γ^2. Thus we only include the vortex

interactions that have the most dramatic impact on the flow: those in which the number of vortices changes. Dritschel and Waugh[26] found that this occurs through either vortex merger, or, if the size disparity between the two vortices is great enough, straining out of the small vortex leading to a loss of its Γ^2. The transformation rule (18) explicitly captures vortex merger while making only small errors in the regime of straining out where r_1/r_2 is small, and hence $\Gamma_1^2 \ll \Gamma_2^2, \Gamma_3^2$. Finally, we neglect the creation of new vortices, which can occur through the rollup of filaments if the ambient strain field is weak enough. This process does occur in turbulent solutions,[2,3] however, its frequency of occurrence is still not well known, and, more importantly, the resulting vortices are relatively small since the antecedent filaments are thin. Hence these vortices have a relatively weak influence on the evolution of the dynamically dominant larger vortices. Thus, in summary, our model consists of point-vortex dynamics, except when same-sign vortices approach closer than d_c (19), at which point they instantaneously merge according to the transformation rules (17) and (18).

B. Renormalization

We are interested in the asymptotic scaling regime of the evolution, after all transients have died away. If there were no limits on computer time or memory, we could start with an enormous number of vortices, and after the transients died away there would still be a large number of vortices and a very long scaling regime, allowing us to accurately average out the sampling fluctuations. With current computers, however, it is not possible to use enough vortices to achieve this accuracy. To overcome this limitation we have developed a renormalization technique, in which the final state of an integration containing few vortices is used to create a new initial state with many more vortices. By integrating over many renormalization cycles we can reach the asymptotic scaling regime and obtain enough data to reduce the sampling error to a reasonable level.

The renormalization procedure starts with a state containing N vortices, with radii r_i. From this state, the procedure produces a new state, where each vortex is copied m times, resulting in $N'=mN$. To remain consistent with scaling theory, Eqs. (5) and (6), each copy must have a new radius $r_i' = r_i m^{-1/4}$, while the vorticity amplitude remains constant. This process can be thought of as using scaling theory to produce, from a state at time t, a state at an earlier time $t'=tm^{-1/\xi}$. If the system were truly in a scaling regime, and large enough that there was no sampling variability, this procedure would merely rewind the system to a previous state. Here we shall use $m=4$.

It remains to determine the positions of the $4N$ vortices. Because the Hamiltonian dynamics of point vortices is sensitive to the configuration of the vortices,[22] we do not wish to place them completely randomly. Rather, the new configuration is determined by the old one. The vortices evolve in a doubly periodic domain, i.e., the infinite plane is tiled with copies of the basic $(2\pi L)^2$ domain. By shrinking distances by a factor of 2, we obtain a new basic domain with $4N$ vortices: Each old vortex at (x_i,y_i) becomes four new vortices at $(x_i/2+n_x\pi L, y_i/2+n_y\pi L)$ with $n_x,n_y=0,1$. In order to prevent the copies from evolving identically due to the large-scale order, we add small random noise to the new positions. This procedure can obviously be generalized to any m that is the square of an integer.

The renormalization procedure reduces distances between vortices by a factor of $m^{1/2}$, while reducing radii by a factor of $m^{1/4}$. Thus, two vortices that before renormalization were not close enough to merge, may after renormalization merge. The result is that after renormalization there is typically a round of merger that reduces the vortex number. If radii were reduced in proportion to distances, this round of merger would be eliminated, but, for consistency with scaling theory, vorticity amplitudes would also have to be renormalized, changing the time scale of the evolution. This alternative is sufficiently more complicated that we prefer the simpler choice, which, as we shall see below, is successful.

It is important to note that since the renormalization scheme is based on scaling theory, the scaling regime we find in the modified point-vortex model is a demonstration of self-consistency of the scaling hypothesis, rather than an independent confirmation. It does, however, provide an independent determination of the scaling exponent ξ since ξ is not used in the renormalization procedure.

C. Scaling regime

Having defined the Hamiltonian, the transformation rules, and the renormalization procedure, we are now in a position to numerically integrate the modified point-vortex model. The equations of motion (12) are integrated using the package LSODE.[27] The domain is doubly periodic with length 2π. An initial condition consists of 400 vortices with uniform initial radius $r_i=0.08$, circulation $\Gamma_i=\pm 1$, half positive and half negative. This initial radius results in vortices whose total area initially covers approximately 20% of the domain. The vorticity, $\zeta_i=\pm\zeta_a=\pm 49.7=\Gamma_i/\pi r_i^2$, is constant throughout the evolution due to the transformation rule (17). The initial positions of the vortices are random, with the restriction that the vortex momentum (16) be equal to its average over all possible configurations, $\mathbf{P}=0$.[22]

A single cycle consists of evolution from $N=400$ to $N=100$, followed by a renormalization back to $N=400$. Five independent initial conditions were created by using independent realizations of the random initial positions. Each initial condition is integrated for 12 cycles, defining a single trajectory.

Once a trajectory reaches the scaling regime, the distribution of vortex radii will be the same at identical times in successive cycles. The distribution at the beginnings of several cycles, obtained by averaging over the five trajectories, is shown in Fig. 8. By cycle seven the distribution appears to have equilibrated and further variation is from fluctuations due to finite sample size. Note that vortices smaller than those in the initial condition appear due to the renormalization of vortex size. In the analysis of the model,

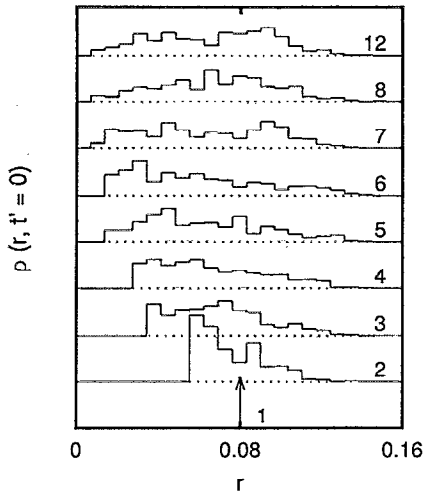

FIG. 8. Probability distribution functions $\rho(r,t')$, $t'=0$, from the modified point-vortex model for several different renormalization cycles, labeled by the numbers on the right. Each distribution is an average over the five independent trajectories. The delta-function initial condition is indicated symbolically by the arrow.

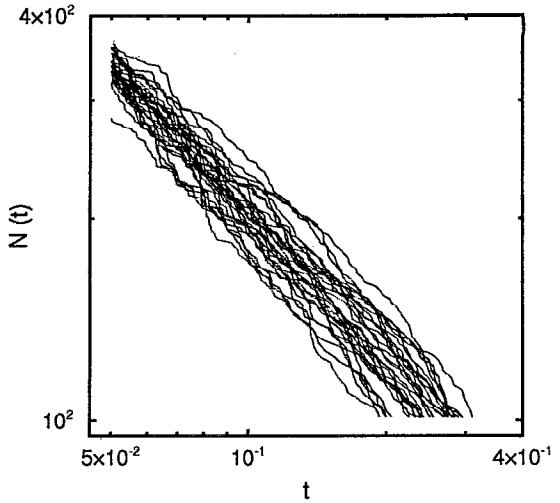

FIG. 9. Vortex number $N(t)$, $t \geqslant t_0$, $t_0=0.050$, for 30 cycles from the modified point-vortex model.

we thus use data from cycles 7–12 from each of the five trajectories, resulting in a total of 30 cycles.

The initial condition for each cycle is defined to occur at $t'=0$, but it is to be considered a state within the scaling regime at some time $t \equiv t'+t_0=t_0$. The hypothesized scaling behavior is (4)–(6). In terms of t', the equation for vortex number, for example, is

$$N(t)=N(t_0)\left(\frac{t'+t_0}{t_0}\right)^{-\xi}. \tag{20}$$

The unknown parameters are thus the exponent ξ, the time t_0, and the values of the average vortex properties at t_0. The only parameter that is relevant for comparison with the turbulence solution in Sec. III is ξ.

The individual cycles exhibit significant variability, both within a single cycle and between cycles, as can be seen in $\rho(r,t)$ (Fig. 8) and $N(t)$ (Fig. 9). To test scaling theory we consider average quantities, denoted by a subscript a. We shall need two different averages: an average over all vortices in a single cycle at a single time, denoted by an overbar; and an average over all cycles at a single time; denoted by angular brackets. Furthermore, the quantities of interest can all be expressed as averages over vortex number and radius:

$$\begin{aligned} N_a(t) &= \langle N(t) \rangle, \\ r_a(t) &= \langle \overline{r_i(t)} \rangle, \\ \Gamma_a(t) &= \pi \zeta_e \langle \overline{r_i^2(t)} \rangle, \\ Z_a(t) &= \frac{\zeta_e^2}{4\pi} \langle N(t) \overline{r_i^2(t)} \rangle, \\ K_a(t) &= 4\pi \left\langle \frac{1}{N(t) \overline{r_i^2(t)}} \right\rangle. \end{aligned} \tag{21}$$

The values of t_0, ξ, and $N(t_0)$ are obtained by performing a least-squares fit of the logarithm of (20),

$$\ln N_a(t) = A - \xi \ln(t'+t_0), \tag{22}$$

where $A \equiv \ln[N(t_0) t_0^{\xi}]$. One can analytically obtain a fit for A and ξ as functions of t_0. A numerical search for the t_0 that minimizes the error completes the fit. Uncertainties are obtained by approximating the fitting error near the minimum as a quadratic function of t_0, and finding the Δt_0 which increases the error by 20%. The results are $t_0=0.050\pm0.003$ and $\xi=0.72\pm0.02$.

The fit of $N_a(t)$ to scaling behavior, shown in Fig. 10, is excellent, indicating that the vortex number does indeed

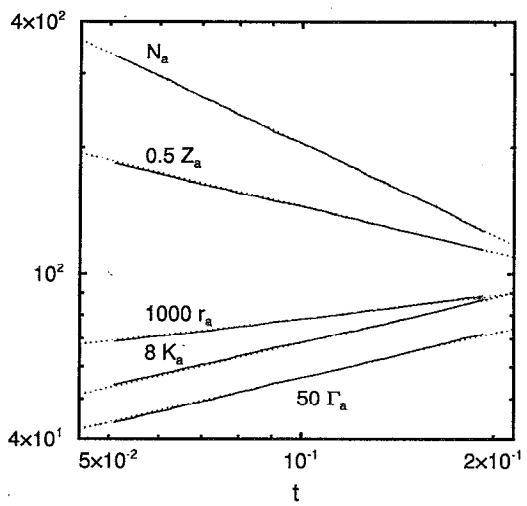

FIG. 10. A comparison of average vortex number $N_a(t)$, vortex radius $r_a(t)$, vortex circulation magnitude $\Gamma_a(t)$, enstrophy $Z_a(t)$, and kurtosis $K_a(t)$ from the modified point-vortex model (solid lines) and scaling theory (dotted lines). In the model, $t_0 \leqslant t \leqslant t_0 + t'_{\text{end}}$, where $t_0=0.050$ and $t'_{\text{end}} \approx 0.14$ is the earliest time for one of the 30 cycles to reach $N=100$.

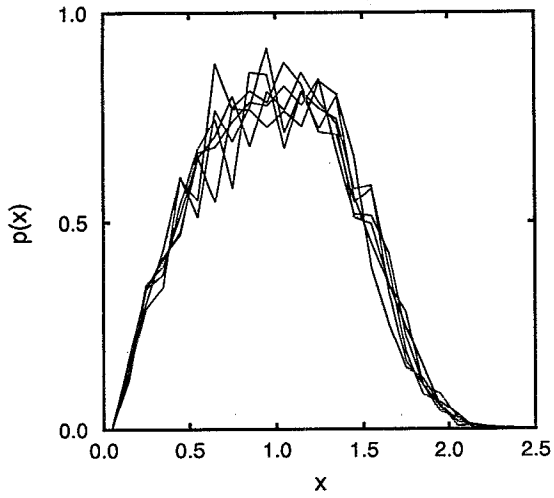

FIG. 11. Probability distribution functions $p(x)$ (9) at six different times from the modified point-vortex model calculated by averaging over the 30 cycles.

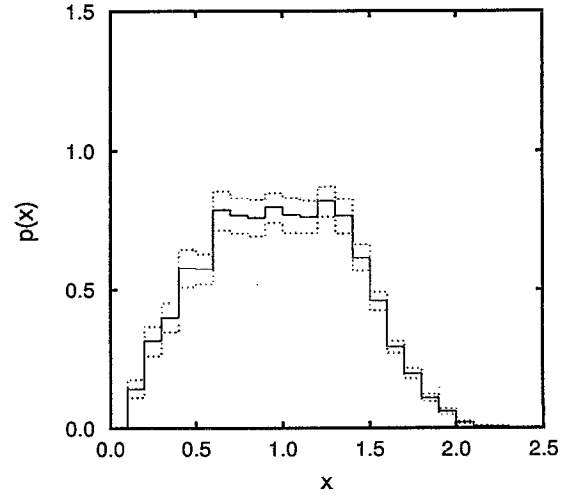

FIG. 12. Best estimate for $p(x)$ (9) from the modified point-vortex model, obtained by averaging over the 30 cycles and over three times within each cycle. The dotted lines indicate the uncertainty estimated by the standard error of the mean, assuming the 90 measurements are independent.

evolve algebraically. Furthermore, the value of ξ found here fits the turbulence solution extremely well (Fig. 1).

A comparison of the other quantities with the scaling theory predictions (6) is also shown in Fig. 10. The values of t_0 and ξ used in the scaling theory predictions are from fitting N_a, while the initial values [$r(t_0)$, etc.] are chosen by requiring the data to match scaling theory at a single intermediate time. The quantities exhibit algebraic evolution, with the exponent well predicted by scaling theory.

The scaling behavior can be interpreted using (21), together with the fact that the transformation rule (18) requires $N(t)\overline{r_i^4}(t)$ be strictly constant for all t and all cycles. Thus, one concludes that $\langle N^\alpha \overline{r_i^\beta}\rangle \sim \langle N\rangle^\alpha \langle \overline{r_i}\rangle^\beta$, from which we infer self-similar evolution of the distribution function, as in (7)–(9). Because all quantities are related by (21) to the vortex number and radius, we focus on the vortex size distribution $\rho(r,t)$, and test the inference that $\rho(r,t)$ evolves as (9).

The distributions at six different times, each obtained by averaging over the 30 cycles, are plotted in Fig. 11. The distributions are, within sampling variability, identical, and one concludes that the hypothesis (9) is true.

The best estimate for $p(x)$ is obtained by averaging over the 30 cycles and several times within each cycle. The behavior of fluctuations leads us to conclude that the correlation time is less than half a cycle. Thus we average over three times: at the beginning, near the middle, and near the end of each cycle. The best estimate for $p(x)$ and its uncertainty are plotted in Fig. 12.

Figures 6 and 11 show that both the modified point-vortex solution and the turbulence solution evolve self-similarly according to (9). Comparison of Figs. 7 and 12, however, shows that the actual shape of $p(x)$ differs significantly between the two, with the point-vortex model containing significantly more small vortices than the turbulence solution. Differences in the large vortex portion of p are small enough to be accounted for by sampling variability.

V. ENERGY PARTITION

The transformation rules for the modified point-vortex model are based on conservation of energy, up to a possible logarithmic correction. Figure 4 shows that the turbulence solution conserves energy extremely well. In this section, we investigate energy conservation in the point-vortex model. In doing so, we formulate an energy partition applicable to any structured flow.

When the vorticity field is structured, one can partition the energy E into three components: the self-energy E_s, the configuration energy E_c, and the background energy E_b. Here E_s, the energy due to self-interaction of the structures, is independent of their positions, while E_c, the interaction energy of the structures, is a function of their spatial configuration. Here E_b is the energy resulting from the nonstructured part of the vorticity, and contains both the interaction between the structures and the background and the self-energy of the background.

The partition is accomplished by rewriting the energy (2) in terms of a Green's function:

$$E=-\frac{1}{2(2\pi L)^2}\int d\mathbf{x}\int d\mathbf{x}'\,\zeta(\mathbf{x})G(\mathbf{x}-\mathbf{x}')\zeta(\mathbf{x}'), \tag{23}$$

where G is defined by

$$\psi(\mathbf{x})=\int d\mathbf{x}'\,G(\mathbf{x}-\mathbf{x}')\zeta(\mathbf{x}'), \tag{24}$$

and translation symmetry requires $G(\mathbf{x},\mathbf{x}')=G(\mathbf{x}-\mathbf{x}')$. Periodic boundary conditions require that the total circulation in the $(2\pi L)^2$ domain be zero. The relation $\nabla^2\psi=\zeta$ then determines the differential equation which G satisfies:

$$\nabla^2 G(\mathbf{x}) = \delta(\mathbf{x}) - \frac{1}{(2\pi L)^2}. \tag{25}$$

Thus, G is the streamfunction resulting from a point vortex with unit circulation, where, to satisfy the requirement on the total circulation, a point vortex is defined as a delta function, together with its compensating uniform vorticity field. Note that in an open domain, $L \to \infty$, and the compensating field vanishes. From previous work on point vortices in a periodic domain,[22] it is known that G is given by (14).

Consider a vortex structure $\hat{\zeta}_i(\mathbf{x})$, with circulation $\Gamma_i = \int d\mathbf{x}\, \hat{\zeta}_i(\mathbf{x})$. The requirement that the total circulation be zero implies that the physical vorticity resulting from a structure is $\zeta_i(\mathbf{x}) = \hat{\zeta}_i(\mathbf{x}) - \Gamma_i/(2\pi L)^2$. The total vorticity can be decomposed into structures and background, $\zeta = \Sigma_i \zeta_i + \zeta_b$, where the background vorticity ζ_b is defined to be whatever vorticity is not accounted for by the structures. The energy partition is then

$$E_s \equiv -\frac{1}{2(2\pi L)^2} \sum_i \int d\mathbf{x} \int d\mathbf{x}'\, \zeta_i(\mathbf{x}) G(\mathbf{x}-\mathbf{x}') \zeta_i(\mathbf{x}'),$$

$$E_c \equiv -\frac{1}{2(2\pi L)^2} \sum_{i,j,i\neq j} \int d\mathbf{x} \int d\mathbf{x}'\, \zeta_i(\mathbf{x}) G(\mathbf{x}-\mathbf{x}') \zeta_j(\mathbf{x}'), \tag{26}$$

$$E_b \equiv -\frac{1}{2(2\pi L)^2} \left(\int d\mathbf{x} \int d\mathbf{x}'\, \zeta_b(\mathbf{x}) G(\mathbf{x}-\mathbf{x}') \zeta_b(\mathbf{x}') + 2 \sum_i \int d\mathbf{x} \int d\mathbf{x}'\, \zeta_i(\mathbf{x}) G(\mathbf{x}-\mathbf{x}') \zeta_b(\mathbf{x}') \right),$$

and $E = E_s + E_c + E_b$.[28]

For the case where the structures are small uniform disks and $\zeta_b = 0$, the lowest-order contributions to the energy components can be found analytically. The structures are described by a size $r_i \ll L$, a vorticity $\hat{\zeta}_i$, and thus a circulation $\Gamma_i = \hat{\zeta}_i \pi r_i^2$. The energy components are then, to lowest order,

$$E_s = -\frac{1}{2(2\pi L)^2} \sum_i \Gamma_i^2 \left[\frac{1}{4\pi} \ln\left(\frac{r_i^2}{2L^2}\right) - \frac{1}{8\pi} - G_c \right],$$

$$E_c = -\frac{1}{2(2\pi L)^2} \sum_{i,j,i\neq j} \Gamma_i \Gamma_j G(\mathbf{x}_i - \mathbf{x}_j), \tag{27}$$

$$E_b = 0.$$

Note that E_c is equal to the point-vortex Hamiltonian (13) divided by $(2\pi L)^2$, the area of the domain. A system of small disk vortices evolving under point-vortex dynamics conserves the total energy since E_c is proportional to the conserved Hamiltonian, and E_s depends only on Γ_i and r_i, which are unaffected by point-vortex dynamics. Note also that in the point-vortex limit, $r_i \to 0$, $\hat{\zeta}_i \to \infty$, with Γ_i remaining constant, E_c is unchanged while E_s becomes infinite.

In the modified point-vortex model the vortex properties evolve due to the transformation of close same-sign vortices. We can see from (27) that the transformation rules used, (17) and (18), equivalent to $\Sigma_i \Gamma_i^2$ being constant, do not strictly conserve E. The nonconservation is, as stated earlier, due to logarithmic terms in E: the term in E_s that depends on r_i, and E_c, which is approximately logarithmic in the vortex separations due to the form of G. The degree of energy nonconservation in the modified point-vortex model is seen in Fig. 13. We also note that an earlier analysis of a single vortex merger event in a spectral model shows transformation of energy from E_c to E_s with no change in E or E_b.[24,28] However, the behavior of a single few-body merger event does not necessarily apply to the variety of many-body merger events found in a turbulent environment.

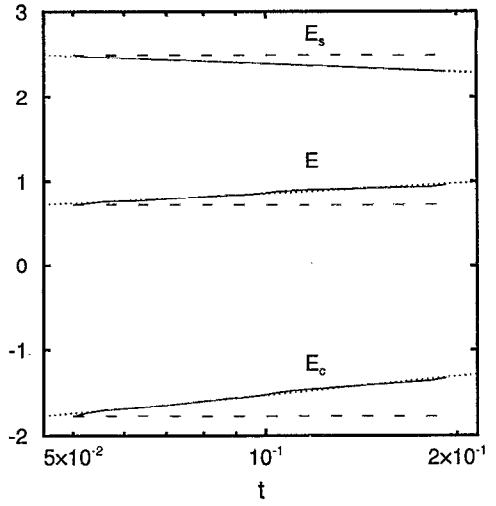

FIG. 13. Energy components E_s, E_c, and total energy E, from the modified point-vortex model, averaged over the 30 cycles. The dotted lines are fits of (30), while the dashed lines are reference lines at constant energy.

The scaling of the energy components (27) with the average vortex properties can be determined using a mean-vortex approximation. The assumptions of this approximation are

$$\sum_i \Gamma_i^2 = aN\Gamma_a^2,$$

$$\sum_i \Gamma_i^2 \ln\left(\frac{r_i}{L}\right) = bN\Gamma_a^2 \ln\left(\frac{r_a}{L}\right), \tag{28}$$

$$\sum_{i,j,i\neq j} \Gamma_i \Gamma_j G(\mathbf{x}_i - \mathbf{x}_j) = -\frac{c}{2} N\Gamma_a^2 G(\mathbf{x}_a),$$

where a, b, c, are positive $O(1)$ constants, and $|\mathbf{x}_a| = 2\pi L/\sqrt{N}$ is a typical nearest-neighbor vortex separation. The scaling of the sum over vortex pairs is due to the fact that N vortices have $N/2$ more opposite-sign pairs than same-sign pairs. Evaluating G using the leading term in a small $\mathbf{x}$ expansion gives

$$E_s = \frac{N\Gamma_a^2}{2(2\pi L)^2} \left[a\left(G_c + \frac{1}{8\pi} + \frac{1}{4\pi} \ln 2 \right) - \frac{b}{2\pi} \ln\left(\frac{r_a}{L}\right) \right],$$

$$E_c = \frac{N\Gamma_a^2 c}{2(2\pi L)^2} \left(\frac{1}{4\pi} \ln \frac{2\pi^2}{N} - G_c \right). \tag{29}$$

Scaling theory, (5) and (6), then gives the time evolution as

$$E_s=E_s^0-c_1 \ln t, \quad c_1>0,$$
$$E_c=E_c^0+c_2 \ln t, \quad c_2>0, \tag{30}$$
$$E=E_s+E_c=E_s^0+E_c^0+(c_2-c_1)\ln t.$$

The assumption (28) with a, b, and c positive results in c_1 and c_2 being positive, and thus predicts that the self-energy decreases with time due to growing r_a/L while the configuration energy grows due to increasing vortex separation caused by decreasing N.

Thus the mean-vortex approximation together with scaling theory predict that the energy components of the modified point-vortex model evolve logarithmically in time. This is seen to be true in Fig. 13, where the energy components are calculated from (27) and averaged over the 30 cycles. Note that $c_2/c_1=2c/b>1$ for the modified point-vortex model; thus the logarithmic increase of energy is a consequence of the distribution functions of vortex size and separation, as manifested in (28).

VI. DISCUSSION

In this paper we have presented results from both a long-time integration of the fluid equations (1) and from a modified point-vortex model that formulates turbulence as a collection of interacting coherent structures. The two systems show excellent agreement in a number of aspects, both with each other and with the mean-vortex scaling theory: the evolution of average vortex properties and low-order moments displays self-similar evolution with the same scaling form. Furthermore, the two systems give the same value of the scaling exponent $\xi\approx 0.72$. Thus, we believe we have achieved and demonstrated a significant degree of understanding of the statistical dynamics of two-dimensional turbulence.

In the turbulence solution, departures of average properties from scaling theory can be rationalized by including finite-Re corrections in the scaling theory. The *ad hoc* functional form of these corrections is algebraic, and the associated exponent η is an incompletely understood function of Re that represents the combined effects of advective straining and viscous diffusion.[29] The corrections do, however, qualitatively capture the relatively small departures from the $\mathrm{Re}=\infty$ scaling theory.

The value of ξ obtained here is consistent with recent laboratory experiments, which also used narrow-band initial conditions.[12] The agreement between three such diverse systems suggests that the value of ξ is universal over some class of initial conditions, within which scaling behavior is approached asymptotically in time. The size of this class is an open question, but we suspect that it is quite large.

There are two significant discrepancies between the modified point-vortex model and the turbulence solution: the shape of the self-similar distribution function $p(x)$ and the behavior of the energy. The fact that our model keeps more small vortices than the turbulence solution, Figs. 7 and 12, leads us to believe that our transformation rules do not adequately capture the dissipative interaction of disparate size vortices. Nonconservation of energy in the model, (29) and Fig. 13, indicates that the transformation rule for vortex size, based on an approximation to the energy that neglects logarithmic variations, is too simple. Thus, both discrepancies can be traced to deficiencies in the characterization of the dissipative interactions.

As shown in (9), self-similarity can occur with any distribution function $p(x)$. Thus, it is not necessarily surprising that the model can capture scaling behavior with the correct ξ, despite the above discrepancies. Furthermore, in our previous work[6] we obtained scaling behavior with roughly the same value of ξ by using a different critical merger distance function, one that resulted in a $p(x)$ that contains even more small vortices. In addition, Carnevale[30] has found that particles that merge using our transformation rules when close, and move not with point-vortex dynamics but as random walkers or with ballistic trajectories, show a wide range of values for ξ, depending on the details of the motion. Carnevale also found that drastically changing the transformation rule so that it conserves Γ rather than Γ^2 affects the value of ξ. From all of this we conclude that $p(x)$ is strongly dependent on the characterization of the dissipative interactions, while ξ depends weakly on at least some aspects of the dissipative transformations but is sensitive to the characterization of the conservative phase of the dynamics.

The deficiencies in the model suggest several directions for improvement. Whereas currently merger of same-sign vortices is the only dissipative process in the model, one could include straining destruction, where small vortices of either sign are destroyed when they get too close to a large vortex. This would have the effect of reducing the number of small vortices, perhaps enough to give the correct $p(x)$. In addition, one could use the more detailed equations for the energy components (27) to construct energy conserving transformation rules. Finally, one could increase the generality of the model by including vortices with unequal amplitudes.

Overall, however, we feel that our strategy of representing two-dimensional decaying turbulence by a simple model containing coherent structures governed by Hamiltonian dynamics and punctuated by abrupt dissipative transformations has been a successful one. Furthermore, we feel that the mathematical framework of punctuated Hamiltonian dynamics is an attractive vehicle for modeling dynamical systems that have an essential dependence on dissipation that occurs only intermittently, insofar as sufficient dynamical understanding exists to characterize the initiating circumstances and the outcomes of dissipative events to create punctuation rules. Punctuated Hamiltonian dynamics provides an efficient representation of the irreversible trends found in nearly conservative systems by modeling them as abrupt transformations rather than following in detail the evolutionary complexity.

ACKNOWLEDGMENTS

This work grew out of our fruitful collaborations with George F. Carnevale, Yves Pomeau, and William R. Young. We thank Christopher G. Goedde for his help in obtaining the reduction of the elliptical-moment model.

The National Center for Atmospheric Research is sponsored by the National Science Foundation.

APPENDIX: THE ELLIPTICAL-MOMENT MODEL

In this appendix we present the elliptical-moment model[15] and focus on the case of two vortices with equal vorticity but unequal size. The model is a Hamiltonian dynamical system with two independent constants of the motion (apart from the energy), and for two vortices it has an eight-dimensional phase space. By appropriate coordinate transformations the system can be reduced to a four-dimensional Hamiltonian with only a conserved energy, and can then be visualized with a two-dimensional Poincaré surface of section. If the vortices are identical, the additional symmetry makes the system integrable.[15] For unequal vortices, however, the system is nonintegrable and the usual features, such as chaotic regions, islands, KAM curves, and cantori, appear.[31,32] The model is numerically integrated to investigate the boundary between those initial conditions that collapse, where the distance between vortex centroids goes to zero, and those that do not. The boundary provides the critical condition for merger in the modified point-vortex model.

The elliptical-moment model describes a collection N of vortices by a Hamiltonian dynamical system in $4N$ variables: $(x_i,y_i,\lambda_i,\phi_i)$, where (x_i,y_i) is the position of the centroid of vortex i, $\lambda_i=a_i/b_i\geqslant 1$ is its ellipticity, a_i and b_i are, respectively, half the major and minor axes of the ellipse, and ϕ_i is the angle of orientation of the major axis with respect to the x axis. The description of each vortex is completed by the inclusion of two parameters: the vorticity ζ_i and vortex area $A_i=\pi a_i b_i$.

In the above coordinates, the model has a singularity for circular vortices, $\lambda_i=1$, where the orientation becomes undefined. The singularity can be removed by changing variables to $(x_i,y_i,\delta_i,\gamma_i)$, where

$$(\delta_i,\gamma_i)=\sqrt{\frac{A_i(\lambda_i-1)^2}{8\pi\lambda_i}}\,[\cos(2\phi_i),\sin(2\phi_i)]. \tag{A1}$$

This change of variables also puts the system into canonical form (apart from the factor $\Gamma_i=A_i\zeta_i$):

$$\Gamma_i\begin{pmatrix}\dot{x}_i\\ \dot{y}_i\\ \dot{\delta}_i\\ \dot{\gamma}_i\end{pmatrix}=\begin{pmatrix}-\dfrac{\partial H}{\partial y_i}\\ \dfrac{\partial H}{\partial x_i}\\ -\dfrac{\partial H}{\partial \gamma_i}\\ \dfrac{\partial H}{\partial \delta_i}\end{pmatrix}. \tag{A2}$$

The Hamiltonian is

$$\begin{aligned}H=\frac{1}{8\pi}\sum_{i=1}^{N}\Bigg\{&\Gamma_i^2\ln\left(1+\frac{2\pi}{A_i}(\delta_i^2+\gamma_i^2)\right)-\frac{\Gamma_i^2}{2}\\&+\sum_{i,j,i\neq j}^{N}\Gamma_i\Gamma_j\Bigg[\ln R_{ij}^2\\&-\frac{2}{R_{ij}^2}\left(\sqrt{\delta_i^2+\gamma_i^2+\frac{A_i}{2\pi}}\,(\delta_i\cos 2\theta_{ij}+\gamma_i\sin 2\theta_{ij})\right.\\&\left.+\sqrt{\delta_j^2+\gamma_j^2+\frac{A_j}{2\pi}}\,(\delta_j\cos 2\theta_{ij}+\gamma_j\sin 2\theta_{ij})\right)\Bigg]\Bigg\},\end{aligned} \tag{A3}$$

where $\cos\theta_{ij}=(x_i-x_j)/R_{ij}$, $\sin\theta_{ij}=(y_i-y_j)/R_{ij}$, and $R_{ij}^2=(x_i-x_j)^2+(y_i-y_j)^2$.

The system has three continuous symmetries, rotation, and translations in x and y, and thus has three dynamical invariants: the angular impulse,

$$M=\sum_{i=1}^{N}\Gamma_i\left(x_i^2+y_i^2+2(\delta_i^2+\gamma_i^2)+\frac{A_i}{2\pi}\right); \tag{A4}$$

and the global centroid,

$$\mathbf{C}=\sum_{i=1}^{N}\Gamma_i\mathbf{x}_i. \tag{A5}$$

There are, however, only two independent invariants, M and $|\mathbf{C}|^2$. The system can thus be reduced from the $4N$-dimensional phase space to $4N-4$ dimensions. We are interested here in the case $N=2$, and the phase space can be reduced to four dimensions.

We choose the unit of time so $\zeta_i=1$, $A_i=\Gamma_i$, choose the origin of our coordinate system so $\mathbf{C}\equiv 0$, and choose the unit of distance so the larger vortex, defined to be vortex 2, has $A_2=\pi$.

Using $R=R_{12}$ and $\theta=\theta_{12}$ reduces the system to six dimensions. The reduction to four dimensions is accomplished by the coordinate change,

$$\begin{aligned}p_i&=\gamma_i\sin 2\theta+\delta_i\cos 2\theta,\\ q_i&=\gamma_i\cos 2\theta-\delta_i\sin 2\theta,\end{aligned} \tag{A6}$$

where $i=1,2$. The reduced equations of motion are

$$\Gamma_i\begin{pmatrix}\dot{q}_i\\ \dot{p}_i\end{pmatrix}=\begin{pmatrix}\dfrac{\partial H}{\partial p_i}\\ -\dfrac{\partial H}{\partial q_i}\end{pmatrix}, \tag{A7}$$

the Hamiltonian is

$$\begin{aligned}H=\sum_{i=1}^{2}\Bigg[&\frac{\Gamma_i^2}{8\pi}\ln\left(1+\frac{2\pi(q_i^2+p_i^2)}{\Gamma_i}\right)\\&-\frac{\Gamma_1\Gamma_2}{2\pi R^2}p_i\sqrt{q_i^2+p_i^2+\frac{\Gamma_i}{2\pi}}\Bigg]+\frac{\Gamma_1\Gamma_2}{4\pi}\ln R^2,\end{aligned} \tag{A8}$$

and the vortex separation R is a function of the coordinates and the angular impulse:

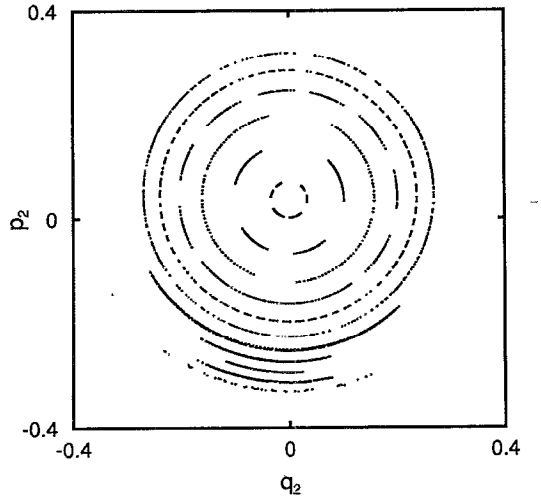

FIG. 14. Poincaré map from numerical integration of the elliptical-moment model containing two vortices with $\Gamma_1=\pi/4$, $\Gamma_2=\pi$, and initial separation $R_0=2.752$.

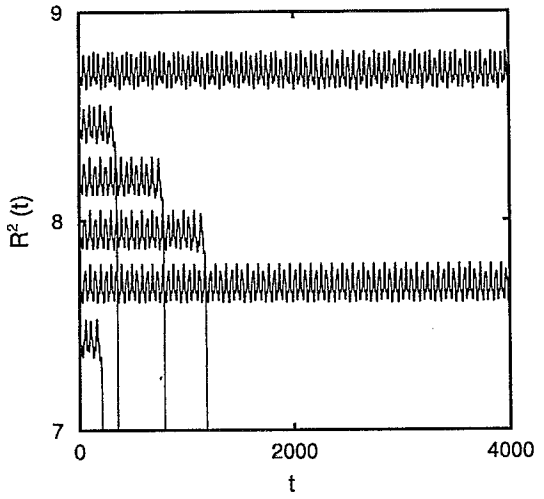

FIG. 15. Vortex separation squared $R^2(t)$ from the elliptical-moment model for initially circular vortices with $\Gamma_1=\pi/4$, $\Gamma_2=\pi$, and initial separations $R_0=2.746$–2.751 in steps of 0.001. The trajectories are successively offset by $\Delta R^2=0.25$.

$$R^2=\frac{\Gamma_1+\Gamma_2}{\Gamma_1\Gamma_2}\left[M-\sum_{i=1}^{2}\left(\frac{\Gamma_i^2}{2\pi}+2\Gamma_i(q_i^2+p_i^2)\right)\right]. \quad \text{(A9)}$$

Note that the Hamiltonian (A8) becomes singular as $R\to 0$.

An initial condition is fully described by the initial vortex shapes (q_1,p_1,q_2,p_2), which are zero for circular vortices, and two parameters, Γ_1 and M. It is convenient to specify the initial vortex separation R_0, which, by (A9), is equivalent to M once the initial shapes are specified. In addition, for circular initial vortices, one can specify the radius r_1 rather than $\Gamma_1=\pi r_1^2$.

The dynamics lies on a three-dimensional energy surface $H=E$ embedded in the four-dimensional phase space, and may be visualized via a two-dimensional Poincaré map. The map we choose is constructed by transforming to action-angle coordinates for vortex 1, $I_1=(q_1^2+p_1^2)/2$, $\tan\alpha_1=q_1/p_1$, and regarding I_1 as a function of the other variables, $I_1=I_1(\alpha_1,q_2,p_2;E)$. We then construct the map with the surface $\alpha_1=0$, oriented with trajectories crossing the surface with increasing α_1.

Figure 14 shows one such Poincaré map for several trajectories, all with the same initial vortex separation but different initial vortex shapes. Trajectories with nearly circular initial conditions (small $q_2^2+p_2^2$ in Fig. 14) are regular and oscillate without collapsing. These regular trajectories, in which the shape and separation of the vortices oscillate as they rotate about each other, are the majority of the trajectories seen in Fig. 14. Trajectories whose initial conditions have sufficiently large ellipticity are in a chaotic region in which collapse occurs. While a chaotic trajectory may spend a significant time trapped by a cantorus, and thus oscillate in a manner similar to a regular trajectory, once the trajectory enters the main chaotic region the vortex separation R rapidly shrinks to zero. The decrease of vortex separation is accompanied by growth in the ellipticity of the vortices, as indicated by Eq. (A9). Because chaotic trajectories collapse so quickly, it is very difficult to show the chaotic region in a Poincaré map. Indeed, the only chaotic trajectory in Fig. 14, the bottom-most arc in the figure, is seen only because it spends some time trapped near an island before escaping and collapsing. As the initial vortex separation decreases, the region of regular oscillations shrinks until the entire phase space is chaotic and all initial conditions collapse.

Defining a simple critical distance d_c, above which vortices never collapse, and below which they always collapse, is not possible due to the complexity of the phase space. For example, it may happen that vortices with one initial separation are inside an island and do not collapse, while vortices initially further apart are in the chaotic region and do collapse. Additionally, the possibility of very long trapping by cantori means that a numerical integration cannot definitively decide whether a particular initial condition will collapse or not. Thus, the critical distance is best thought of as a fuzzy boundary, where well below the boundary vortices collapse rapidly, while well above the boundary they do not collapse.

In practice, however, the width of the boundary region is very small. Figure 15 depicts the vortex separation $R(t)$ for six trajectories containing initially circular vortices with initial separations spanning the boundary region. The spread in initial separations among the trajectories is only 0.2%, across which the behavior varies from no collapse in 4000 time units ($\approx$40 oscillations) to collapse after a few hundred time units. All vortices with initial separations smaller than those in the boundary region will collapse, while vortices with larger separations will not collapse. Note that once collapse begins, the separation very quickly drops to zero.

In defining d_c we restrict ourselves to initially circular vortices, leaving two nondimensional parameters to define the initial condition: the size of the small vortex r_1 and the

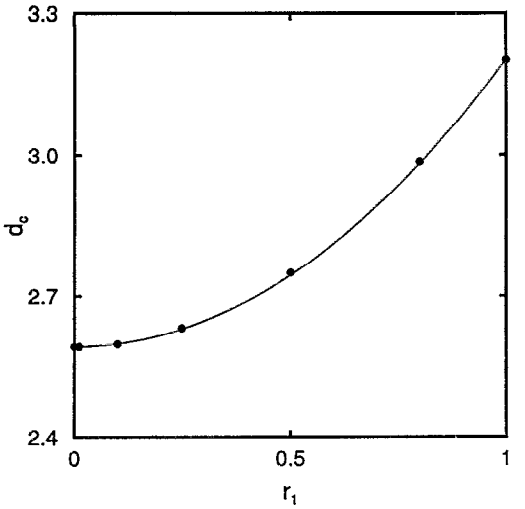

FIG. 16. Nondimensional critical distance $d_c(r_1)$ from the elliptical-moment model. The circles are the largest separation for which initially circular vortices collapse, while the solid line is a parabolic fit, $a+br_1^2$, with $a=2.592$ and $b=0.609$.

initial vortex separation R_0. The complexity of the collapse boundary is sufficiently narrow that for our purposes it can be ignored; we thus define the critical distance $d_c(r_1)$ as the largest value of R_0 for which two initially circular vortices collapse. The results of numerical integrations using a resolution of 0.001 in R_0 fit a quadratic, $d_c(r_1)=a+br_1^2$, $a=2.592$, $b=0.609$, surprisingly well (Fig. 16). It is not yet understood why the complex structure of phase space results in such a simple fit. The dimensional form of d_c is shown in (19).

[1]M. Brachet, M. Meneguzzi, H. Politano, and P. Sulem, "The dynamics of freely decaying two-dimensional turbulence," J. Fluid Mech. **194**, 333 (1988).

[2]P. Santangelo, R. Benzi, and B. Legras, "The generation of vortices in high-resolution, two-dimensional, decaying turbulence and the influence of initial conditions on the breaking of self-similarity," Phys. Fluids A **1**, 1027 (1989).

[3]J. C. McWilliams, "The vortices of two-dimensional turbulence," J. Fluid Mech. **219**, 361 (1990).

[4]W. H. Matthaeus, W. T. Stribling, D. Martinez, S. Oughton, and D. Montgomery, "Selective decay and coherent vortices in two-dimensional incompressible turbulence," Phys. Rev. Lett. **66**, 2731 (1991); W. H. Matthaeus, W. T. Stribling, D. Martinez, S. Oughton, and D. Montgomery, "Decaying, two-dimensional, Navier–Stokes turbulence at very long times," Physica D **51**, 531 (1991).

[5]K. Ohkitani, "Wave number space dynamics of enstrophy cascade in a forced two-dimensional turbulence," Phys. Fluids A **3**, 1598 (1991).

[6]G. F. Carnevale, J. C. McWilliams, Y. Pomeau, J. B. Weiss, and W. R. Young, "Evolution of vortex statistics in two-dimensional turbulence," Phys. Rev. Lett. **66**, 2735 (1991).

[7]G. F. Carnevale, J. C. McWilliams, Y. Pomeau, J. B. Weiss, and W. R. Young, "Rates, pathways, and end-states of nonlinear evolution in decaying two-dimensional turbulence: Scaling theory versus selective decay," Phys. Fluids A **4**, 1314 (1992).

[8]G. K. Batchelor, "Computation of the energy spectrum in homogeneous two-dimensional turbulence," Phys. Fluids Suppl. II, 233 (1969).

[9]J. C. McWilliams, "The emergence of isolated coherent vortices in turbulent flow," J. Fluid Mech. **146**, 21 (1984).

[10]M. Lesieur, *Turbulence in Fluids* (Kluwer Academic, Dordrecht, 1990).

[11]R. Benzi, S. Patarnello, and R. Santangelo, "Self-similar coherent structures in two-dimensional decaying turbulence," J. Phys. A. Gen. **21**, 1221 (1988).

[12]P. Tabeling, S. Burkhart, O. Cardoso, and H. Willaime, "Experimental study of freely decaying two-dimensional turbulence," Phys. Rev. Lett. **67**, 3772 (1991).

[13]J. C. McWilliams, "A demonstration of the suppression of turbulent cascades by coherent vortices in two-dimensional turbulence," Phys. Fluids A **2**, 547 (1990).

[14]M. V. Melander, J. C. McWilliams, and N. J. Zabusky, "Axisymmetrization and vorticity-gradient intensification of an isolated two-dimensional vortex through filamentation," J. Fluid Mech. **178**, 137 (1987).

[15]M. V. Melander, N. J. Zabusky, and J. C. McWilliams, "Symmetric vortex merger in two dimensions: Causes and conditions," J. Fluid Mech. **195**, 303 (1988).

[16]D. G. Dritschel, "Strain-induced vortex stripping," in *Mathematical Aspects of Vortex Dynamics*, edited by R. E. Caflisch (SIAM, Philadelphia, 1989), p. 107.

[17]R. Benzi, M. Colella, M. Briscolini, and P. Santangelo, "A simple point vortex model for two-dimensional decaying turbulence," Phys. Fluids A **4**, 1036 (1992).

[18]R. Benzi, S. Patarnello, and R. Santangelo, "On the statistical properties of two-dimensional decaying turbulence," Europhys. Lett. **3**, 811 (1987).

[19]A. Leonard, "Vortex methods for flow simulation," J. Comput. Phys. **37**, 289 (1980).

[20]N. J. Zabusky, M. H. Hughes, and K. V. Roberts, "Contour dynamics for the Euler equations in two dimensions," J. Comput. Phys. **30**, 96 (1979).

[21]H. Aref, "Integrable, chaotic, and turbulent vortex motion in two-dimensional flows," Annu. Rev. Fluid Mech. **15**, 345 (1983).

[22]J. B. Weiss and J. C. McWilliams, "Nonergodicity of point vortices," Phys. Fluids A **3**, 835 (1991).

[23]The equations in Ref. 22 differ from (13)–(15) in that there they are nondimensional and have $G_c=0$.

[24]J. C. McWilliams and J. B. Weiss, "The search for simplified models of two-dimensional, structured turbulence," in *Nonlinear Phenomena in Atmospheric and Oceanic Sciences*, IMA Volumes in Mathematics and Applications, edited by G. F. Carnevale and R. T. Pierrehumbert (Springer-Verlag, New York, 1992), Vol. 40.

[25]M. V. Melander, N. J. Zabusky, and A. S. Styczek, "A moment model for vortex interactions of the two-dimensional Euler equations. Part 1. Computational validation of a Hamiltonian elliptical representation," J. Fluid Mech. **167**, 95 (1986).

[26]D. G. Dritschel and D. W. Waugh, "Quantification of the inelastic interaction of unequal vortices in two-dimensional vortex dynamics," Phys. Fluids A **4**, 1737 (1992).

[27]A. C. Hindmarsh, in *Scientific Computing*, edited by R. S. Stepleman in collaboration with M. Carver, R. Peskin, W. F. Ames, and R. Vichnevetsky (North-Holland, Amsterdam, 1983), p. 55.

[28]The energy partition used here is different from that in Ref. 24 in that here the compensating vorticity fields required to make the total circulation zero are included in the structured part of the vorticity field, rather than the background. This choice results in the energy components being independent of the value of the arbitrary constant in G.

[29]W. R. Young, P. B. Rhines, and C. J. R. Garrett, "Shear-flow dispersion, internal waves and horizontal mixing in the ocean," J. Phys. Ocean. **12**, 515 (1982).

[30]G. F. Carnevale (private communication, 1991).

[31]A. J. Lichtenberg and M. A. Lieberman, *Regular and Stochastic Motion* (Springer-Verlag, New York, 1983).

[32]R. S. Mackay and J. D. Meiss, *Hamiltonian Dynamical Systems* (Adam Hilger, Bristol, 1987).